

Dynamic High-Order Control Barrier Functions with Diffuser for Safety-Critical Trajectory Planning at Signal-Free Intersections

Di Chen, Ruiguo Zhong, Kehua Chen, Zhiwei Shang, Meixin Zhu*, Edward Chung

Abstract—Planning safe and efficient trajectories through signal-free intersections presents significant challenges for autonomous vehicles (AVs), particularly in dynamic, multi-task environments with unpredictable interactions and an increased possibility of conflicts. This study aims to address these challenges by developing a robust, adaptive framework to ensure safety in such complex scenarios. Existing approaches often struggle to provide reliable safety mechanisms in dynamic and learn multi-task behaviors from demonstrations in signal-free intersections. This study proposes a safety-critical planning method that integrates Dynamic High-Order Control Barrier Functions (DHOCBF) with a diffusion-based model, called Dynamic Safety-Critical Diffuser (DSC-Diffuser), offering a robust solution for adaptive, safe, and multi-task driving in signal-free intersections. Our approach incorporates a goal-oriented, task-guided diffusion model, enabling the model to learn multiple driving tasks simultaneously from real-world data. To further ensure driving safety in dynamic environments, the proposed DHOCBF framework dynamically adjusts to account for the movements of surrounding vehicles, offering enhanced adaptability compared to traditional control barrier functions. Validity evaluations of DHOCBF, conducted through numerical simulations, demonstrate its robustness in adapting to variations in obstacle velocities, sizes, uncertainties, and locations, effectively maintaining driving safety across a wide range of complex and uncertain scenarios. Performance evaluations across various scenes confirm that DSC-Diffuser provides realistic, stable, and generalizable policies, equipping it with the flexibility to adapt to diverse driving tasks.

Index Terms—Autonomous Vehicles, Safety-Critical Control, Generative model, Driving safety, Control Barrier Function.

I. INTRODUCTION

NAVIGATING intersections, particularly, is regarded as complex by most human drivers, as they must decide on a passing time and execute crash-free crossing maneuvers. According to the latest report of the National Highway Traffic Safety Administration (NHTSA) [1] in the United States, in 2022, the number of fatalities at intersections was approximately 12,036, accounting for about 28.31% of the total.

This research is supported by the National Natural Science Foundation of China (NSFC, Grant No.52302379). (Co-responding author: Meixin Zhu)

Di Chen, Edward Chung are with the Department of Electrical and Electronic Engineering of The Hong Kong Polytechnic University, Hong Kong, China (email: di-03.chen@polyu.edu.hk, edward.cs.chung@polyu.edu.hk)

Ruiguo Zhong, Zhiwei Shang, Meixin Zhu are with the Thrust of Intelligent Transportation, The Hong Kong University of Science and Technology (Guangzhou), Nansha, Guangzhou, 511400, Guangdong, China, (email: rzhong151@connect.hkust-gz.edu.cn, zhiweishang@hkust-gz.edu.cn, meixin@hkust-gz.edu.cn)

Kehua Chen is with the Civil and Environmental Engineering Department, The Hong Kong University of Science and Technology (email: kchenbm@connect.ust.hk)

Within them, accidents at unsignalized intersections accounted for 65.07% of the total at intersections. The increasing number of fatalities at unsignalized intersections presents a problem in determining how to navigate them safely for autonomous vehicles (AVs).

There are three driving tasks in signal-free intersections: turning left, going straight, and turning right. From the perspective of the task, the existing research on signal-free intersection planning can be divided into two categories: single- [2] and multi-task [3] using synthesise [4], [5] or real-world network [6]. Given the safety-critical nature of these scenarios, this study addresses multi-task learning and safety-critical trajectory planning for AVs at signal-free intersections on real-world roads, where complex vehicle movements arise from a highly interactive environment. In this context, the main challenges are as follows: 1) how to learn multi-tasks at different conditions. 2) how to make safety-critical trajectory planning in the complex scene.

A popular choice for trajectory planning at signal-free intersections for autonomous vehicles has been heuristic-based methods for their stability, interpretability, and ability to handle constraints explicitly [7]. However, its predefined rules make it difficult to adapt well to the dynamic and complex environment. Learning-based methods have been prevalent in autonomous driving for their ability to deal with complex scenarios. Reinforcement learning (RL) models learn by interacting with the environment through exploration and exploitation guided by reward functions. However, these policies may not exhibit natural behavior, leading to difficulties in situations that require human-like driving behavior to coordinate with other agents and adhere to driving conventions [8]. Moreover, poorly designed reward functions can lead to unintended or unsafe actions [9]. Learning to drive from demonstrations has gained significant attention, as it enables agents to learn human-like policies and eases the reward design burden in RL [8]. Many imitation methods assume a uni-modal action distribution, which causes problems when training with multi-modal expert demonstrations of various tasks. Recently, diffusion models have been shown to account for diverse and complex behaviors, making them well-suited for learning from multi-modal demonstrations [10].

In terms of safety, guaranteeing the planner's safety using these methods alone is challenging. This is because these models are trained on datasets or simulations, making them unable to cope with previously unseen environments and situations. Control Barrier Functions (CBFs) are effective in

maintaining safety in the presence of bounded disturbances [11] when the obstacles are immobile. Dynamic CBFs [12] have been introduced to avoid moving obstacles, but they are implemented in discrete-time systems. The control system for AVs in this study is a 2nd-order and continuous-time system requiring High-Order CBF (HOCBF) [13]. Our approach extends HOCBFs to make them adaptive and less conservative, achieving safe driving in continuous-time and dynamic signal-free intersections.

This study addresses the challenge of enabling vehicles to learn various tasks, such as turning left, going straight, and turning right, while developing safety-critical planning strategies for crossing signal-free intersections. The contributions of this study can be summarized as follows:

- 1) A safety planning framework is proposed, in which an integration of trajectory generation and safety modifier has been developed to learn human-like and safety-critical driving policies for left turns, right turns, and going straight at signal-free intersections.
- 2) A task-guided and goal-oriented generation method is first introduced into signal-free intersections to recover policies from Interaction Datasets [14].
- 3) Dynamic HOCBF (DHOCBF) is proposed to serve as a hard constraint to ensure that the ego vehicle remains within the safe set through set invariance in a dynamic environment. This method can be also involved in other frameworks.
- 4) The performance of the proposed dynamic safety-critical diffuser (DSC-Diffuser) algorithm has been evaluated by comparing it with state-of-the-art algorithms and human driving trajectory data. Additionally, comparisons in two distinct scenarios are conducted to demonstrate the model's strong generalization capability and safety.

The paper is structured as follows. Section II provides a literature review of related research. Section III elaborates on task-guided and goal-oriented planning methods using Diffuser, the derivation of the DHOCBF, and the formulation of the control system and safety controller. Section IV presents the experimental settings, the Interaction dataset [14], data processing details for signal-free intersections, and the comparison algorithms and evaluation metrics. Section V includes the results and discussion of the comparison experiments. The conclusions are drawn in Section VI.

II. LITERATURE REVIEW

A. Trajectory Planning Methods in Signal-Free Intersections

In signal-free intersections trajectory planning, the existing studies can be classified into four groups: heuristic-based methods, RL, imitation learning (IL), and generative methods.

Heuristic-based methods are often used to tackle these problems, designed for connected autonomous vehicles by cooperative control [7], [15], [16], [17], [18], [19]. These methods aim to optimize joint control and enhance safety by leveraging predefined rules and strategies. However, a notable limitation of these methods is their tendency to overlook the influence and uncertainties associated with human drivers.

Moreover, the development of effective heuristics often demands significant domain expertise and manual effort.

RL agents can learn optimal policies for AVs by interacting with the environment. This allows them to dynamically adjust to varying traffic conditions and uncertainties. [20] proposed an automated curriculum for Proximal Policy Optimization (PPO) to accelerate the training of agents in signal-free intersections. [21] modeled autonomous driving at intersections as a Markov Decision Process combined RL with hierarchical options to consider the uncertainties in planning. They set a goal to guide vehicles to complete different tasks, but the performance was worst in left-turn scenarios. [22] implemented a layered structure featuring an RL-based decision planner at the high level and an MPC controller at the lower level. However, this framework does not address scenarios where the ego-vehicle may need to execute left or right turns at intersections, rather than simply proceeding straight. [23] proposed a predictive trajectory planning framework for AVs using deep Q learning, with input graphs capturing driving scenarios, to ensure safe, comfortable, and energy-efficient navigation. [24] designed a hierarchical RL framework for left-turn policies at signal-free intersections. However, many of these methods are tailored for single-task execution. Moreover, most of them are trained in simulation and enforce safety constraints by shaping the reward functions of RL rather than using hard constraints, making it difficult to guarantee safety in complex or unseen scenarios.

Learning from demonstration enables agents to perform tasks by mimicking human behavior from datasets that implicitly capture interactions without the need for hand-crafted designs. Data availability encourages the adoption of IL methods that do not require interaction with the environment (i.e., off-policy methods such as behavior cloning). However, these methods can result in distribution shifts and causal confusion [25], which can be tackled by closed-loop training. [26] proposed a conditional imitation learning with an Occupancy Grid Mapping (OGM) method to avoid static road blockages on single-lane roads. In [27], a model-based generative adversarial imitation learning (MGAIL) technique was introduced to provide flexibility in specifying new goals and to generalize beyond observed expert trajectories in urban self-driving environments. However, this method exhibits limitations in generalizing to novel routes and underperforms in challenging scenarios. [28] presented a hierarchical imitation learning approach to generate executable trajectories and cost maps, enhancing the reliability and stability of AVs driving. However, these methods are still not collision-free.

Traditional generative models, such as Generative Adversarial Networks (GANs), leverage noise variables to model variations, while Variational Autoencoders (VAEs) focus on capturing underlying trajectory distributions. However, these methods face limitations in fully capturing the complex dynamics of driving behavior. Recently, diffusion models have been widely applied in trajectory planning [29] due to their potential to synthesize rich, complex behaviors from multimodal demonstrations. [30] proposed reward-guided denoising to facilitate task optimization with non-differentiable objectives combined with large language models. To facilitate

generative planning and data synthesis in multi-task offline settings, [31] combined diffusion with transformer backbones and prompt learning. An intention-aware diffusion model [32] separates trajectory uncertainty into goal and action uncertainties, modeling them with two interconnected diffusion processes. These studies have proved that diffusion has great potential for multi-task and uncertainty learning in complex environments. While these studies showed strong potential in generating complex, realistic behaviors, the explicit safety mechanisms have been overlooked, which is paramount for AVs in dynamic and uncertain traffic environments. Our work leverages a diffusion model with goal-setting and task guidance to enable multi-task planning in complex, signal-free intersections while incorporating an additional module to ensure safe driving.

B. Safety Critical Control for Trajectory Planning

In practice, any trajectory planning policies require additional safety measures to enforce hard constraints for collision avoidance. Safety-critical control is typically achieved through constraint-handling methods, including optimal control and CBFs.

[33] introduced future-focused control barrier functions (ff-CBF) to reduce the conservatism of CBF for AVs at signal-free intersections. [34] proposed a trajectory tracking method by relaxing the CBF constraint to the cost function without using optimization processes. [35] presented the parametric CBF by proposing a polynomial \mathcal{K} function to capture different behaviors of homogeneous drivers in merging scenarios. Constraint-Guided Diffusion (CGD) [36] combines diffusion policies with a surrogate optimization scheme within an imitation learning framework, efficiently generating collision-free and dynamically feasible trajectories. [37] proposed the SafeDiffuser model by incorporating a class of CBFs to ensure collision-free diffusion data generation. [38] introduced a Restoration Gap Guidance (RGG) to adjust and improve unsafe trajectories produced by diffusion planners. Some other studies [39], [40] have combined traditional CBFs with learning-based methods to maintain safety in autonomous driving. However, these constraints either consider only static environments or overlook the dynamic behavior of surrounding vehicles, limiting their effectiveness in real-world traffic scenarios. CBFs are typically designed to address static obstacles, focusing on maintaining safety relative to fixed objects without accounting for the movement and interaction of other vehicles. Consequently, using traditional CBFs in autonomous driving can lead to overly conservative or unsafe decisions [12], especially in complex, unpredictable traffic conditions.

Therefore, this study proposes DHOCBF as a hard constraint to account for the dynamics of surrounding vehicles, ensuring safe navigating through signal-free intersections.

III. METHODOLOGY

Navigating signal-free intersections presents unique challenges in urban traffic due to the absence of traffic signals, requiring vehicles to adapt to dynamic and uncertain environments. This section details our problem formulation and

the methodology used to generate human-like trajectories and ensure safe navigation at such intersections.

A. Problem Formulation

Our algorithm is specifically designed for navigating signal-free intersections, which are common in urban traffic environments and present unique challenges due to the absence of traffic signals. Unlike scenarios such as lane changing on a highway, in this context, the location of the target position after crossing is known. The problem is formulated as the conditional-generating problem. Specifically, suppose $\mathcal{F}(\cdot)$ is our model, which generates the human-like trajectories using the initial and end positions, along with the task as conditions.

$$\tau = \mathcal{F}(s_t, a_t, s_{t+H}, \mathcal{M}, S_{obs}(t)) \quad (1)$$

where the trajectory τ consists of a sequence of states and actions:

$$\tau := (s_t, a_t, s_{t+1}, a_{t+1}, \dots, s_{t+H}, a_{t+H}) \quad (2)$$

where t denotes the time at which a state was visited in trajectory, and the state is defined as $s_t := (x_t, y_t, v_{x_t}, v_{y_t})$. The action at time t is defined as $a_t := (a_{x_t}, a_{y_t})$. H denotes the trajectory horizon, and s_{t+H} denotes the end position regarded as the planning goal. The task \mathcal{M} , which can take one of three values, corresponds to different maneuvers: $\{TurningLeft, GoingStraight, TurningRight\}$, represented by $-1, 0$, and 1 , respectively. $S_{obs}(t)$ is the set of states of other vehicles which are regarded as obstacles for the ego vehicle and $S_{obs}(t) := \{s_{obs}^1(t), s_{obs}^2(t), \dots, s_{obs}^N(t)\}$. N is the number of surrounding vehicles within the sensory range set as 8 meters [41]. In each planning step t' , the state of the ego vehicle is updated by:

$$s_{t'}, a_{t'} = \mathcal{F}(O_{t'}, \tau_{t'-1} | s_{t+H}, \mathcal{M}) \quad (3)$$

where t' is the planning time, and $t < t' < t + H$. In this study, task-guided and goal-oriented diffusion models are used to recover policies from human driver datasets at signal-free intersections. Subsequently, the output of the diffusion models is used as a reference control, and DHOCBF is incorporated as a hard constraint to ensure driving safety, as shown in Fig. 1.

B. Task-Guided and Goal-Oriented Planning with Diffuser

At signal-free intersections, distinct trajectory plans are necessary for left turns, right turns, and straight ahead. To distinguish between these separate tasks during the planning, classifier-free guidance can infuse task information as conditions (encoded in $\mathcal{I}(\tau)$) into the diffusion process. Diffusion model [42] learns by reversing a controlled diffusion process, which consists of two main stages: a forward diffusion stage $q(\tau^j | \tau^{j-1})$ and a backward denoising stage $p_\theta(\tau^{j-1} | \tau^j, \mathcal{I}(\tau))$. Then the posterior distribution of the diffusion process from τ^0 to τ^T is formulated as:

$$q(\tau_{1:N} | \tau^0) := \prod_{j=1}^N q(\tau^j | \tau^{j-1}) \quad (4)$$

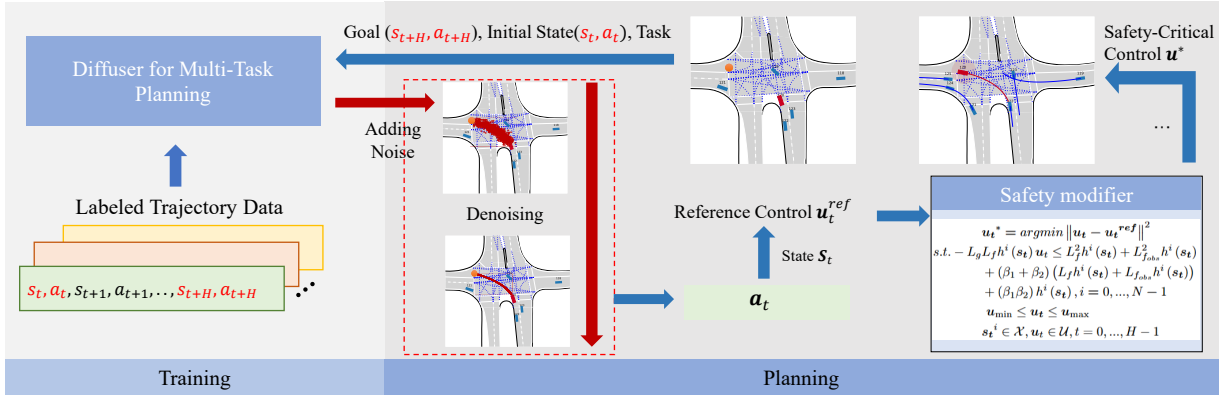


Fig. 1. The framework of the DSC-Diffuser planner. In the training process, the labeled data are used to train the diffuser for multi-task learning. The blue arrows represent the planning process of the proposed DSC-Diffuser in horizon H , while the red arrows represent the generation process in the Diffuser. The orange point is the goal.

Correspondingly, the reverse diffusion process is given by:

$$p(\tau_{0:N}|\mathbf{l}(\tau)) := p(\tau_N) \prod_{j=1}^N p_{\theta}(\tau^{j-1}|\tau^j, \mathbf{l}(\tau)) \quad (5)$$

where $p(\tau_N)$ is an initial noise Gaussian distribution.

Distinct from classifier guidance, the unconditional denoising diffusion model p_{θ} parameterized through a score estimator $\epsilon_{\theta}(\tau^j)$ is trained together with the conditional model $p_{\theta}(\tau^j|\mathbf{l}(\tau^i))$ parameterized through $\epsilon_{\theta}(\tau^j, \mathbf{l}(\tau))$. The score of classifier-free guidance [43] is defined as:

$$\tilde{\epsilon} = \epsilon_{\theta}(\tau^j, \emptyset, j) + w\epsilon_{\theta}(\tau^j, \mathbf{l}(\tau), j) - w\epsilon_{\theta}(\tau^j, \emptyset, j) \quad (6)$$

where w is the guidance scale. In this work, there are two types of timesteps: one associated with the diffusion process and the other with the planning process. To maintain clarity, superscripts $j \in \{1, \dots, T\}$ denote timesteps in the forward diffusion stage, while subscripts $t \in \{1, \dots, H\}$ indicate the trajectory timesteps. When $w = 0$, the conditional information has no impact on trajectory generation, whereas larger values of w can significantly strengthen this influence. Also, unreasonable results may be obtained if the guidance weight w is too high. Then, the loss function can be defined as [43]:

$$\mathcal{L}(\theta) = \mathbb{E}_{j, \tau, \epsilon} \left[\|\epsilon - \epsilon_{\theta}(\tau^j, (1-\beta)\mathbf{y}(\tau^j) + \beta\emptyset, j)\|^2 \right] + \mathbb{E}_{a, \tau^j} [\|a - a'(\tau^j)\|^2] \quad (7)$$

where β represents the probability of ignoring the conditional information, ϵ denotes the sample noise in the forward process, and a denotes the action set of the trajectory in the dataset. When crossing the intersection, a constraint is required to ensure the generation of feasible trajectories that terminate at a goal location. Referring to [44], the constraint of the state is defined as:

$$C(\tau) = \begin{cases} +\infty & \text{if } \mathbf{g}_t = (s_t, \mathbf{a}_t) \\ 0 & \text{otherwise} \end{cases} \quad (8)$$

where \mathbf{g}_t is the goal set of state and action at time t . To implement this constraint, the sampled values are replaced by the goal \mathbf{g}_t after all diffusion timesteps i .

C. Safety-Critical Planning by DHOCBF

To design a safety-critical controller, an affine control system in the following form is considered:

$$\dot{s}_t = f(s_t) + g(s_t)u_t \quad (9)$$

where $s_t \in \mathbb{R}^n$, $f: \mathbb{R}^n \rightarrow \mathbb{R}^n$, $g: \mathbb{R}^n \rightarrow \mathbb{R}^{n \times q}$ are locally Lipschitz continuous, and $u_t \in U \subset \mathbb{R}^q$ where U denotes a control constraint set.

Definition 1. (Set invariance) A set $C \subset \mathbb{R}^n$ is forward invariant for system 9 if its solutions for some $u \in U$ starting at any $s_0 \in C$ satisfy $s_t \in C$, $\forall t > 0$. A safe set is defined as $C = \{s_t \in \mathbb{R}^n \mid h(s_t) \geq 0\}$, where $h: \mathbb{R}^n \rightarrow \mathbb{R}$ is a continuously differentiable function.

Definition 2. (Barrier Function, BF) The function $h: \mathbb{R}^n \rightarrow \mathbb{R}$ is a candidate BF for system 9 if there exists a class \mathcal{K} function α such that:

$$\dot{h}(s) + \alpha(h(s)) \geq 0, \quad \forall s \in C. \quad (10)$$

Definition 3. (Control Barrier Function, CBF [45]) A function $h(s_t)$ is a candidate control barrier function for a system if there exists an extended class \mathcal{K} function α such that:

$$\sup_{u \in U} [L_f h(s_t) + L_g h(s_t)u] \geq -\alpha(h(s_t)) \quad (11)$$

where L_f and L_g represent the Lie derivatives along the functions f and g , respectively. The set of all input u that satisfy Eq.11 for s_t can be defined as:

$$K_{cbf}(s_t) = \{u \in U : L_f h(s_t) + L_g h(s_t)u + \alpha h(s_t) \geq 0\} \quad (12)$$

Then, a differential control system model for driving is defined:

$$\begin{bmatrix} \dot{x}_t \\ \dot{y}_t \\ \dot{v}_{x_t} \\ \dot{v}_{y_t} \end{bmatrix} = \begin{bmatrix} v_{x_t} \\ v_{y_t} \\ 0 \\ 0 \end{bmatrix} + \begin{bmatrix} 0 & 0 \\ 0 & 0 \\ 1 & 0 \\ 0 & 1 \end{bmatrix} \begin{bmatrix} u_{x_t} \\ u_{y_t} \end{bmatrix} \quad (13)$$

where $s_t := (x_t, y_t, v_{x_t}, v_{y_t})$, $u_t = (u_{x_t}, u_{y_t})$, x_t, y_t denote the horizontal and vertical movement of vehicle, v_{x_t}, v_{y_t} denote the vertical and lateral speeds, u_{x_t}, u_{y_t} denote the control inputs for vertical and lateral acceleration. Vertical

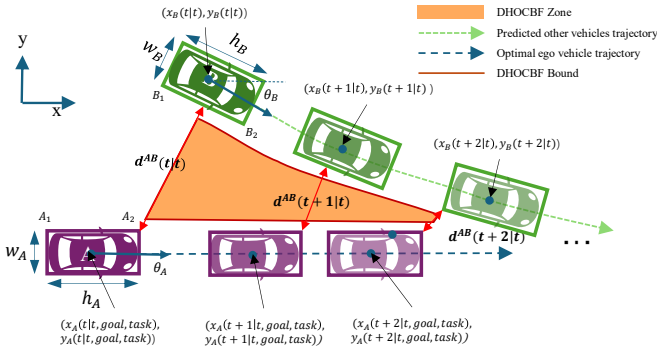


Fig. 2. The optimal trajectory for ego vehicle A $p_A(t : t + H|t)$ to avoid a collision with other vehicle B $p_B(t : t + H|t)$, whose trajectory is predicted, at time t over H future steps. The safe distance, $d_{safe}^i(t)$, is dynamic. The HOCBF zone is the safe region, limited by HOCBF bounds, ensuring $h(s_t, s_{obs}^i(t)) \geq 0$, so that the ego vehicle A does not approach the other vehicle B too closely.

and lateral directions are the directions of movement along the lane and perpendicular to the lane. The barrier function $h(s_t, s_{obs}^i(t)) = (x_t - x_{obs}^i(t))^2 + (y_t - y_{obs}^i(t))^2 - (d_{safe}^i(t))^2$, where $i = 0, 1, \dots, N-1$. In previous research, obstacles and vehicles are typically modeled as ellipses or circles [33]. Given the limited space at signal-free intersections, representing vehicles as ellipses or circles can significantly lead to deadlock maneuvers [46]. Each vehicle can be represented as a rectangle, described by the position $p^i(t) = (x^i(t), y^i(t))$ and additional information $l^i(t) = (w^i, h^i, \theta^i(t))$, as shown in Fig.2.

$d_{safe}^i(t)$ is the minimum and dynamic safe distance between the other vehicle i and ego vehicle at time t . Initially, the two closest points on the surfaces of the two vehicles are identified. The minimum distance between the corner of the rectangle and the surface of the other rectangle can be calculated by Eq.14. The position of the point in the surface is determined by Eq.15. Subsequently, the projection of the line segment formed by these points onto the centerline is calculated. Ultimately, the minimum safe distance is derived. As the vehicle travels approximately at the original angle for a brief period, the effect of angular acceleration on the minimum safe distance is neglected in the derivation; thus,

$$d_{min}^{B_1 A_1 A_2} = \begin{cases} \left| \frac{\overrightarrow{A_1 B_1} \cdot \overrightarrow{A_1 A_2}}{|\overrightarrow{A_1 A_2}|} \right|, r \geq 1 \\ \left| \frac{\overrightarrow{A_2 B_1} \cdot \overrightarrow{A_1 A_2}}{|\overrightarrow{A_1 A_2}|} \right|, r \leq 0 \\ \left| \frac{\overrightarrow{A_1 B_1} \cdot \overrightarrow{A_1 A_2}}{|\overrightarrow{A_1 A_2}|} \cdot \sin(|\theta_A - \theta_B|) \right|, \text{otherwise} \end{cases} \quad (14)$$

$$p_{surf} = \begin{cases} A_1, & r \geq 1 \\ A_2, & r \leq 0 \\ (x_{A_1} + r \cdot (x_{A_2} - x_{A_1}), \\ y_{A_1} + r \cdot (y_{A_2} - y_{A_1})), & \text{otherwise} \end{cases} \quad (15)$$

where $r = \frac{\overrightarrow{A_1 B_1} \cdot \overrightarrow{A_1 A_2}}{|\overrightarrow{A_1 A_2}|^2}$.

Condition 11 ensures that if $h(x) \geq 0$, the system's state will remain within the safe set C for all future times. Based on Eq.13, the CBF is calculated, and it is found that

$L_g s_t = 0$, indicating that the control input u_t is unable to ensure system safety. Our control system exhibits 2nd-order dynamics, therefore standard CBFs may not be sufficient. High Order Control Barrier Functions (HOCBFs) [47] extend the concept of CBFs to include higher-order derivatives of the safety function $h(x)$, thereby allowing for more robust safety guarantees.

Definition 4 (High Order Control Barrier Function (HOCBF) [13]) A function $b: \mathbb{R}^n \times [t_0, \infty) \rightarrow \mathbb{R}$ is a candidate HOCBF for affine control system if it is m th-order differentiable and there exist differentiable class \mathcal{K} functions $\alpha_i, i \in \{1, \dots, m\}$ s.t.

$$\gamma_m(s_t) \geq 0 \quad (16)$$

for all $(s_t) \in C_1(t) \cap \dots \cap C_m(t) \times [t_0, \infty)$. And, $\gamma_i(s_t) = \dot{\gamma}_{i-1}(s_t) + \alpha_i \gamma_{i-1}(s_t), i \in \{1, \dots, m\}, C_i(t) = \{s_t \in \mathbb{R}^n : \gamma_{i-1}(s_t) \geq 0\}, i \in \{1, \dots, m\}$. $\gamma_0(s_t) = h(x_t)$. α_i denotes class \mathcal{K} functions.

In dynamic CBF, $h(s_t, s_{obs})$ is defined as a barrier function that incorporates information about the opponent's vehicle; thus

$$\dot{h}(s_t, s_{obs}) = \frac{\partial h(s_t, s_{obs}(t))}{\partial s_t} \dot{s}_t + \frac{\partial h(s_t, s_{obs}(t))}{\partial s_{obs}(t)} \dot{s}_{obs}(t) \quad (17)$$

By Nagumo's theorem, given a continuously differentiable constraint $h(s_t, s_{obs}(t))$ ($h(s_0, s_{obs}(t)) \geq 0$) and combining with 16, the necessary and sufficient condition for guaranteeing the forward invariance of the safe set C is:

$$\gamma_m(s_t, s_{obs}(t)) \geq 0, \forall s_t \in C_1(t) \cap \dots \cap C_m(t) \quad (18)$$

α_1 and α_2 are linear and equal to β_1 and β_2 , which are constants. In a dynamic environment, other vehicles are beyond our control, thus $u_{obs} = 0$. It is assumed that all vehicles have the same control system model and information about the state of the opponent's vehicle can be obtained at each time step. Therefore, the 2nd-HOCBF constraint Eq.[13] is reformulated for a dynamic environment as follows. Here $h(s_t, s_{obs}^i(t))$ is abbreviated to $h(s_t)$.

$$\begin{aligned} -L_g L_f h(s_t) u_t &\leq L_f^2 h(s_t) + L_{f_{obs}}^2 h(s_t) \\ &\quad + (\beta_1 + \beta_2) (L_f h(s_t) + L_{f_{obs}} h(s_t)) \\ &\quad + (\dot{\beta}_1 + \beta_1 \beta_2) h(s_t) \end{aligned} \quad (19)$$

where

$$\begin{aligned} L_g L_f h(s_t) &= [2(x_t - x_t^o), 2(y_t - y_t^o)] \\ L_f^2 h(s_t) &= 2v_t^2, \\ L_f h(s_t) &= 2(x_t - x_t^o)v_{x_t} + 2(y_t - y_t^o)v_{y_t}, \\ L_{f_{obs}}^2 h(s_t) &= 2v_{obs}^2(t), \\ L_{f_{obs}} h(s_t) &= -2(x_t - x_t^o)v_{x_t}^o - 2(y_t - y_t^o)v_{y_t}^o. \end{aligned} \quad (20)$$

In the given equations, $z = x$ represents the input to the model, $\beta_1(z), \beta_2(z)$ are the adjustable parameters. The value of $\dot{\beta}_1(z)$ is fixed at 0. Combined with the objective function, the safety controller can be modeled:

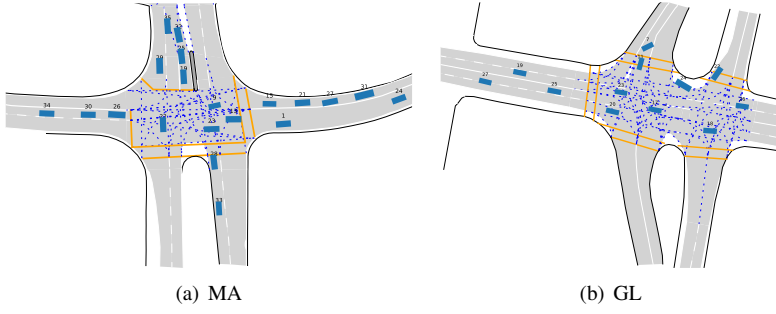


Fig. 3. MA and GL scenarios for given situations. The orange lines are stop lines and pedestrian lines.

$$\begin{aligned}
 \mathbf{u}_t^* &= \operatorname{argmin} \|\mathbf{u}_t - \mathbf{u}_t^{ref}\|^2 \\
 s.t. - L_g L_f h^i(\mathbf{s}_t) \mathbf{u}_t &\leq L_f^2 h^i(\mathbf{s}_t) + L_{f_{obs}}^2 h^i(\mathbf{s}_t) \\
 &+ (\beta_1 + \beta_2) (L_f h^i(\mathbf{s}_t) + L_{f_{obs}} h^i(\mathbf{s}_t)) \\
 &+ (\beta_1 \beta_2) h^i(\mathbf{s}_t), i = 0, \dots, N-1 \\
 \mathbf{u}_{\min} &\leq \mathbf{u}_t \leq \mathbf{u}_{\max} \\
 \mathbf{s}_t^i &\in \mathcal{X}, \mathbf{u}_t \in \mathcal{U}, t = 0, \dots, H-1
 \end{aligned} \tag{21}$$

where \mathbf{u}_t^{ref} denotes the reference control of trajectories, which is calculated by the output of the planner $\mathbf{u}^p(t)$ and current state \mathbf{s}_t to make our safe trajectories close to the reference trajectories of planner, and \mathcal{X}, \mathcal{U} are the sets of admissible states and inputs, respectively. Using the following quadratic program (QP)-based controller design, the input \mathbf{u}_t^{ref} given by the global planner can be minimally modified by the input \mathbf{u}^* that satisfies Eq.19. It is important to note that the safety controller acts more like a safety modifier.

IV. EXPERIMENTS

The experimental settings, dataset, and data processing are first described. Subsequently, the assessment metrics and comparison algorithms are presented. A series of experiments in the same and a different signal-free intersections, distinct from the training scenario, are conducted to demonstrate the effectiveness and generalization of our approach by comparing it with other algorithms, including rule-based and imitation learning methods.

A. Datasets

Our framework is evaluated using the Interaction dataset [14], which provides naturalistic motion data from diverse traffic participants across various highly interactive driving scenarios in different countries. Data from two unsignalized intersection scenarios in the USA (GL and MA) are used, as shown in Fig.3 and TABLE I. This study addresses the trajectory planning problem for crossing signal-free intersections while disregarding the stop-line crossing rule. Thus, trajectories between the point of crossing the pedestrian line and the pedestrian line at the target intersection are intercepted. All models are trained in the MA scene, which includes approximately 230 trajectories for each movement: turning

TABLE I
THE SUMMARY OF THE DATA

Scenarios	Number of vehicles	Video length (min)
MA	2982	107.37
GL	10518	259.43

right, going straight, and turning left. Two experiments are conducted to assess model performance and generalization: one in the MA scene, the same as the training scene, and another in the GL scene, which is distinct. Notably, all algorithms use the same processed, collision-free trajectory data.

B. Comparison Algorithms

- 1) *Human driver*: The data from Interaction dataset [14].
- 2) *IDM*: The Intelligent Driver Model (IDM) calculates acceleration based on the current speed and the gap to the leading vehicle. Referring to [48], the closest vehicle that lies within 8 meters of the ego's planned path and with a heading difference of less than 15° is chosen as the leader vehicle. This model poses challenges in these driving scenarios, where it is unclear which vehicle the ego should "follow". A desired speed of 9.63 m/s, a minimum spacing of 2.5 m, a desired time headway of 1.6s, a nominal acceleration of 2.0 m/s^2 , and a comfortable braking deceleration of 3.0 m/s^2 are set. All parameter values are referenced to Interaction datasets [14] and [49].
- 3) *BC*: Behavior Cloning (BC) [50] method mimics a subset of the dataset via supervised learning, which is implemented to regress features to a mean and standard deviation that parameterize a normal distribution for ego vehicle acceleration. The model was trained by minimizing the negative log-likelihood of expert actions.
- 4) *GAIL*: Generative Adversarial Imitation Learning (GAIL) aims to infer the latent reward function from the dataset and derive the driving policy by optimizing the learned reward. The agent is trained using the optimization objective and PPO as described in [51].
- 5) *SHAIL*: Safety-Aware Hierarchical Adversarial Imitation Learning (SHAIL) [48] builds on GAIL by introducing high-level option selection to enhance safety. Details of this algorithm can be found in [48].
- 6) *DSC-Diffuser*: The proposed DSC-Diffuser method is used to learn policies from datasets and maintain safety. To explore the roles of task guidance, goal orientation, and DHOCBF, ablation experiments are conducted.

C. Metrics

Average Displacement Error (ADE), Final Displacement Error (FDE), and success rate (SR) [25] are used to demonstrate

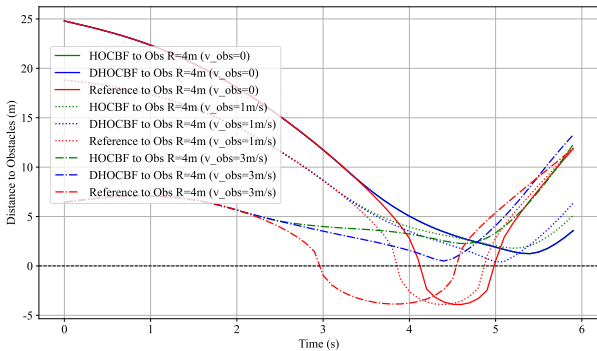
the realism of our approach in comparison to human drivers and to assess the safety of these planning methods. The SR is defined as the ratio of the number of non-colliding trajectories to the total number of trajectories. Since the positions of the last step as the goals are used in the DSC-diffuser, the FDE of the algorithm's output is fixed at zero. Therefore, the displacement error of the penultimate step is used as the FDE for the DSC-diffuser.

V. RESULTS AND DISCUSSION

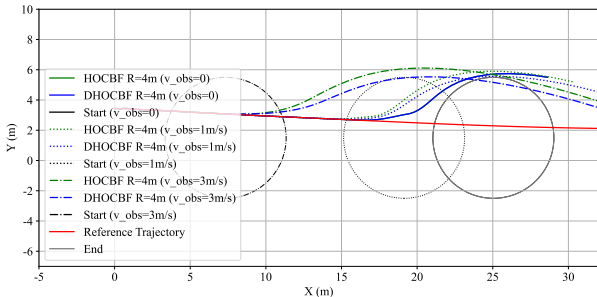
In this section, the effectiveness of DHOCBF is first validated in maintaining safety within dynamic environments by comparing it with HOCBF under various conditions. Then, to further evaluate the effectiveness of the proposed DSC-Diffuser method, a comparison was conducted with other baseline methods in the same scenarios. Additionally, different guidance strengths, as well as the use of DHOCBF and goal setting, were tested to demonstrate the role of each module. All experimental results were obtained from five independent trials, each using a different random seed, to ensure statistical evidence. The average values from the tests in the MA and GL are shown in TABLE II and TABLE III, respectively.

A. Validity Experiment of DHOCBF

To demonstrate the adaptability of the proposed DHOCBF in dynamic environments, its ability to ensure safety is verified in scenarios with different obstacle velocities (Fig.4), varying



(a) Distance to Obstacles Over Time for HOCBF and DHOCBF with Varying Obstacle Speeds



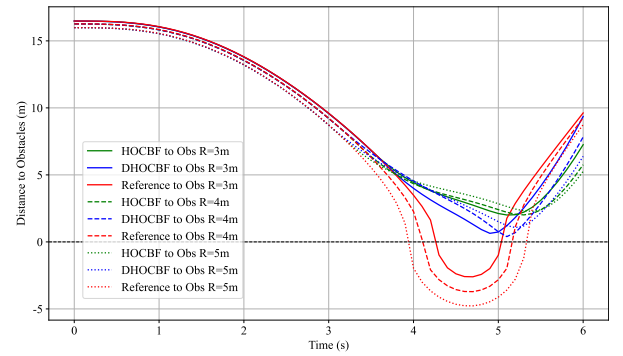
(b) Generated Trajectories of HOCBF and DHOCBF with Varying Obstacle Speeds

Fig. 4. Performance Comparison of HOCBF and DHOCBF with Dynamic Obstacles of Varying Speeds. The speed of obstacles is set as 0, 1 m/s , 3 m/s . In this case, the ego vehicle is traveling in the same direction.

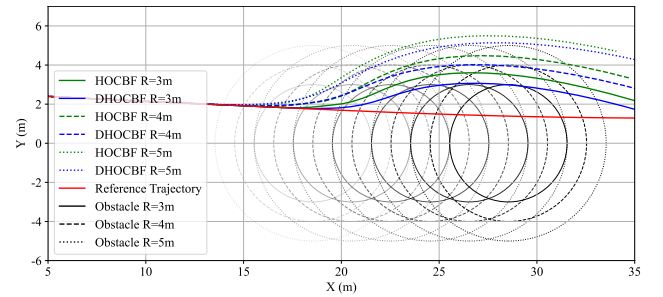
obstacle sizes (Fig.5), environmental perturbations (Fig.6), and multiple obstacles (Fig.7), by comparing it with HOCBF. For clearer visualization, obstacles are simplified to circles, and the size of the ego vehicle is disregarded, so any distance greater than 0 is considered safe. Infeasible reference trajectories are provided, allowing the distance to obstacles to reflect the safety and conservatism of the two constraints, HOCBF and DHOCBF. The distances between the ego vehicle and obstacles are shown in Fig.4(a), Fig.5(a) and Fig.7(a). The trajectories of reference and HOCBF-generated and DHOCBF-generated are shown in Fig.4(b), Fig.5(b), Fig.6 and Fig.7(b).

The direction of motion of the original trajectory is from left to right. The original trajectory is nearly aligned with the positive X direction, with speeds consistently greater than 5.2 m/s . Additionally, to represent the movement of an obstacle, multiple circles are used, where lighter colors indicate earlier positions over time. Both the obstacles and the ego vehicle start moving from time 0, except in Fig.6. The optimal values β_1 and β_2 of K functions are found by repeated experiments such that the quadratic programs(QPs) are feasible and the barrier function $h(x)$ is minimized when the constraints first become active. The optimal value varies under various conditions of HOCBF and DHOCBF.

- 1) Fig.4(a), Fig.5(a) and Fig.7(a) show that both DHOCBF-generated and HOCBF-generated trajectories are safe when the ego vehicle and obstacles travel in the same direction under different conditions, as the distances to obstacles are consistently greater than 0. These results



(a) Distance to Obstacles Over Time for HOCBF and DHOCBF with Varying Radii



(b) Generated Trajectories of HOCBF and DHOCBF in Multi-Obstacle Scenarios

Fig. 5. Comparative Analysis of HOCBF and DHOCBF with Varying Obstacle Radii. The obstacles move at a speed of 2 m/s in the positive x -direction.

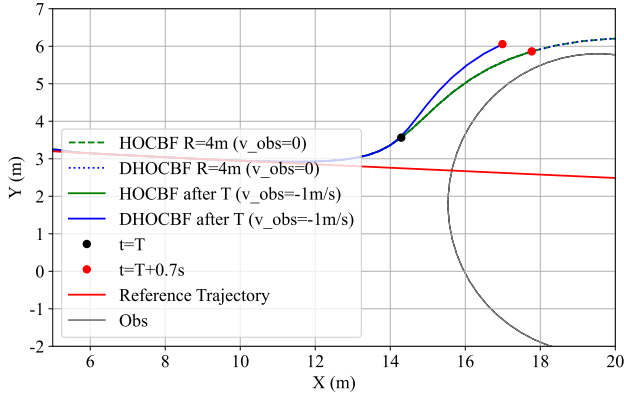
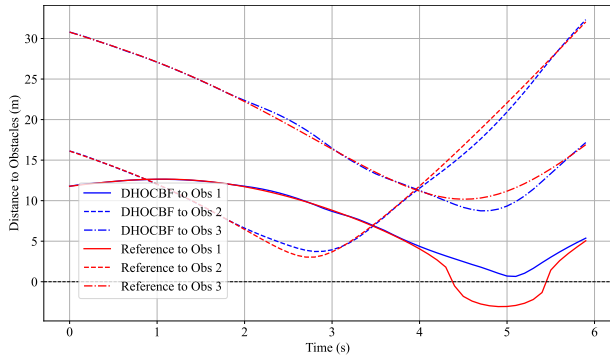
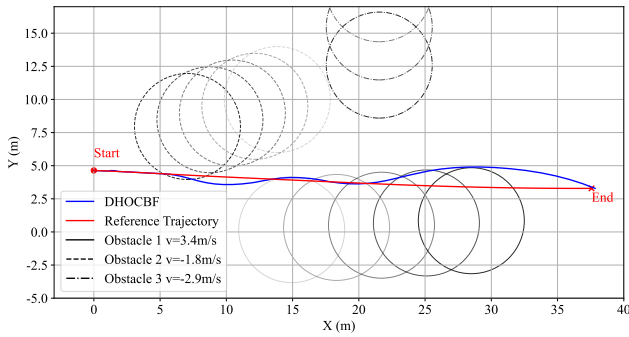


Fig. 6. Generated Trajectories of HOCBF and DHOCBF under Environmental Disturbance. Initially, the obstacle is stationary, and at time T , it is assigned a velocity of $v = -1 \text{ m/s}$, representing the uncertainty from the environment. The position of the obstacle here is the position at time T .



(a) Distance to Obstacles Over Time



(b) Generated Trajectories of DHOCBF in Complex Scenarios

Fig. 7. Distance to Obstacles and Generated Trajectories of the DHOCBF in Complex Scenarios

demonstrate that trajectories generated by HOCBF and DHOCBF can adapt to variations in obstacle velocity and size.

- 2) When comparing the trajectories in Fig.4(a) and Fig.4(b), the gap between the HOCBF-generated trajectory and the reference trajectory increases with obstacle speed, highlighting HOCBF's conservatism in dynamic environments. The DHOCBF-generated trajectories more closely follow the reference trajectory, while maintaining smaller safe distances to the obstacle and demonstrating DHOCBF's adaptability to dynamic environments, avoiding overly conservative behavior.

- 3) In Fig.6, the response of two constraints to environmental perturbations is demonstrated. When the obstacle is stationary without perturbations, both HOCBF and DHOCBF produce the same trajectories. At the time T , after the obstacle's velocity changes to -1 m/s (opposite to the ego vehicle's direction of driving) from 0, the DHOCBF-generated trajectory adjusts to maintain a greater distance from the obstacle, whereas the HOCBF-generated trajectory remains unchanged as if the obstacle were stationary. DHOCBF demonstrates the ability to maintain driving safety in uncertain environments, exhibiting robustness to perturbations.
- 4) DHOCBF is robust in a complex environment, as shown in Fig.7, which presents the safe trajectory navigating 3 surrounding objects.

B. Performance Evaluation in MA Scene

Among baseline methods, BC demonstrates relatively high error rates, with an ADE of 8.8202 and FDE of 5.9210, indicating limitations in generalization from the training data. GAIL improves upon BC, achieving lower error rates (ADE of 7.4530 and FDE of 4.1321), suggesting that adversarial training enhances performance. However, GAIL's high variance in ADE (1.1900) and FDE (0.6506) indicates inconsistencies in predictions. SHAIL maintains a relatively high SR of 0.8989, but with ADE and FDE values of 10.2724 and 5.8210, respectively, it doesn't substantially outperform BC in accuracy. IDM performs the poorest among baseline models, with the highest error rates (ADE of 10.7766 and FDE of 6.5177), reflecting its inadequacy in complex, dynamic environments.

The diffuser model without goals and task guidance performs better than the baseline models, showing the ability of the diffuser model to learn diverse behavior from multiple tasks in expert demonstrations. As guidance weight increases from 0 to 8, ADE decreases from 3.8868 to 1.7410, while FDE reduces from 2.5057 to 1.6712. Variability in ADE and FDE (VAR_ADE and VAR_FDE) also drops significantly, from 2.0382 to 0.1367 and 0.3802 to 0.0294, respectively, as guidance weight rises. These results highlight the effectiveness of guidance in enhancing multi-task learning capabilities in complex environments and improving stability. The SR also reaches its peak of 1 at a guidance weight of 8, although it slightly decreases to 0.9512 when the guidance weight is raised to 16, indicating that more guidance may offer diminishing returns. Similar performance trends are observed across other metrics, underscoring the role of task guidance in maximizing the model's effectiveness.

In contrast, diffuser with goals demonstrates superior accuracy, consistency, and safety across all guidance weights. At a guidance weight of 0, the diffuser with goals achieves an ADE of $4.27\text{E-}06$ and FDE of 0.002048, with variances in ADE and FDE at nearly zero ($3.01\text{E-}14$ and $1.85\text{E-}08$, respectively), indicating exceptional stability. Unlike the diffuser model without goal, where performance improves with increased guidance, adding more guidance to the diffuser with goals decreases its performance. This likely occurs because once a specific goal is defined, the task objectives are already

TABLE II
THE VALUES OF COMPARISON METRICS IN MA SCENE

MA												
	Guidance	ADE	VAR_ADE	FDE	VAR_FDE	SR		ADE	VAR_ADE	FDE	VAR_FDE	SR
BC	-	8.8202	0.3985	5.9210	0.2053	0.7879	-	-	-	-	-	-
GAIL	-	7.4530	1.1900	4.1321	0.6506	0.8687	-	-	-	-	-	-
SHAIL	-	10.2724	1.7157	5.8210	1.0354	0.8989	-	-	-	-	-	-
IDM	-	10.7766	0	6.5177	0	-	-	-	-	-	-	-
Diffuser w/o Goals	0	3.8868	2.0381	2.5057	0.3802	0.9756	DSC-Diffuser w/o Goals	3.7689	1.6556	2.4544	0.2964	1
	3	2.6204	0.3832	1.9497	0.0627	0.9756		2.5886	0.3152	1.9568	0.0589	1
	5	2.0798	0.5939	1.6859	0.1223	0.9512		2.1296	0.6338	1.7345	0.1316	1
	8	1.7410	0.1367	1.6712	0.0294	0.9756		1.7833	0.1439	1.7182	0.0316	1
	10	2.7616	0.3692	2.0893	0.1318	1		2.5162	0.2615	1.9846	0.0826	1
	16	2.0539	0.1415	1.9431	0.0285	0.9512		1.9626	0.1566	1.8751	0.0230	1
	21	3.6321	1.5530	2.4490	0.0163	0.9756		3.6810	2.3388	2.4412	0.0527	1
Diffuser w/ Goals	0	4.27E-06	3.01E-14	0.002048	1.85E-08	1	DSC-Diffuser w/ Goals (ours)	5.43E-06	2.70E-14	0.002544	1.73E-08	1
	3	4.82E-06	2.26E-14	0.002057	1.48E-08	1		5.99E-06	3.25E-14	0.002567	1.14E-08	1
	5	6.31E-06	1.28E-13	0.002287	3.49E-08	1		7.49E-06	1.25E-13	0.002781	3.75E-08	1
	8	1.13E-05	1.37E-12	0.003084	1.48E-08	1		1.25E-05	1.44E-12	0.003527	1.95E-08	1
	10	1.46E-05	9.32E-13	0.003482	1.33E-07	1		1.58E-05	1.05E-12	0.003877	1.08E-07	1
	16	3.08E-05	1.03E-11	0.004687	2.17E-07	1		3.28E-05	1.16E-11	0.005211	5.94E-08	1
	21	4.15E-05	3.75E-12	0.005519	1.94E-07	1		4.31E-05	4.33E-12	0.005860	2.43E-07	1

embedded within the initial state and the goal itself, rendering additional guidance redundant and potentially disruptive. This behavior highlights the efficiency of the goal, as it enables the model to achieve optimal performance without the need for guidance of tasks, showcasing its robustness in accurately and reliably reaching designated targets. In this scenario, DSC-Diffuser exhibits only minor changes that slightly reduce model performance by incorporating DHOCBF, due to the already high SR achieved by the diffuser with goals. This indicates that the model's intrinsic stability and safety metrics are robust under the trained scenario.

C. Performance Evaluation in GL Scene

In the untrained GL scenario, the ADE and FDE values for all algorithms are substantially increased. The ADE and FDE values for BC, GAIL, and SHAIL all exceed 20 and 10 meters, respectively, reflecting their low generalizability and potential inadequacy in unseen environments.

In the diffuser without goals model, setting a guidance weight of 3 achieves the lowest ADE of 8.5744, showing a marked improvement in accuracy compared to setting 0, which has an ADE of 9.2155. However, as the settings increase to 21, the ADE rises to 11.3702, indicating diminishing returns and potential overfitting at higher settings. Similarly, the FDE follows a comparable pattern, with setting 3 achieving a lower FDE of 5.1510 compared to setting 0's FDE of 5.2785 but rising to 5.7141 at setting 21. This trend is similar in the MA scene, while the best guidance weight varies from scenes.

The diffuser with goals model and DSC-Diffuser consistently maintain a low ADE around 0.0433 and 0.0408 across all settings, respectively, demonstrating superior accuracy compared to the diffuser without goals models and

other models. Without DHOCBF, this performance stability is complemented by a consistently high SR of 0.9756 in the diffuser with goals model, highlighting the effectiveness of goal-oriented modeling in maintaining both generalization and reliability.

In this scene, incorporating DHOCBF not only maintains driving safety by improving SR values but also reduces the ADE and FDE values in the two diffuser-based models. For example, the diffuser without goals and guidance yields ADE, FDE, and SR values of 9.125, 5.2785, and 0.8537, respectively, whereas the DSC-Diffuser without goals improves these values to 9.3565, 5.1551, and 1. The DSC-Diffuser decreases ADE and FDE from 0.0434 to 0.0408 and from 0.0285 to 0.0276, and increases SR from 0.9756 to 1, compared to the diffuser with goals.

VI. CONCLUSION

This paper proposes a multi-task learning and safety-critical planning method based on a diffusion model to recover policies from expert demonstrations with various tasks while proposing and incorporating DHOCBF as a hard constraint to maintain driving safety. The main findings and conclusions can be summarized as follows:

- 1) DHOCBF demonstrates robust adaptability to variations in obstacle speeds, sizes, uncertainties, and positions, ensuring driving safety in dynamic, complex, and uncertain environments.
- 2) Adjusting guidance weights can enhance model performance in scenarios without defined goals, though optimal weights vary by scenario and condition. Excessive guidance may lead to diminishing returns and potential overfitting. However, task guidance has minimal impact

TABLE III
THE VALUES OF COMPARISON METRICS IN GL SCENE

GL											
	Guidance	ADE	VAR_ADE	FDE	VAR_FDE	SR		ADE	VAR_ADE	FDE	SR
BC	-	20.3496	0.4589	10.9258	0.2772	0.7931	-	-	-	-	-
GAIL	-	21.6658	3.2296	10.2060	0.7223	0.8103	-	-	-	-	-
SHAIL	-	24.9691	1.8091	12.5948	1.2626	0.8987	-	-	-	-	-
IDM	-	23.8632	0	11.2839	0	-	-	-	-	-	-
Diffuser w/o Goals	0	9.2155	0.5191	5.2785	0.0447	0.8537	DSC-Diffuser w/o Goals	9.3565	0.2489	5.1551	0.0272
	3	8.6467	0.2496	5.1510	0.0264	0.9024		8.6949	0.6293	4.9581	0.0354
	5	8.7930	0.2096	5.1477	0.0323	0.8780		8.5104	0.5525	4.8757	0.0972
	8	8.5744	0.1750	5.0771	0.0109	0.9024		7.9324	0.1784	4.7465	0.0157
	10	8.9708	0.2845	5.1656	0.0414	0.8049		7.8013	0.4111	4.7753	0.0367
	16	10.0141	0.8819	5.4722	0.1003	0.8049		9.3768	0.4779	5.2218	0.0489
	21	11.3702	5.4213	5.7141	0.4488	0.8537		9.7676	3.8147	5.2103	0.3478
Diffuser w/ Goals	0	0.0434	7.08E-09	0.0285	1.39E-07	0.9756	DSC-Diffuser w/ Goals (ours)	0.0408	1.08E-08	0.0276	1.50E-07
	3	0.0434	5.93E-09	0.0288	1.07E-07	0.9756		0.0408	9.03E-09	0.0278	1.30E-07
	5	0.0433	1.29E-08	0.0287	9.77E-08	0.9756		0.0408	2.07E-08	0.0277	1.18E-07
	8	0.0433	9.83E-09	0.0290	2.98E-07	0.9756		0.0407	1.64E-08	0.0281	2.76E-07
	10	0.0433	1.38E-08	0.0292	1.99E-07	0.9756		0.0408	1.64E-08	0.0282	2.10E-07
	16	0.0432	4.74E-08	0.0296	2.72E-07	0.9756		0.0407	5.00E-08	0.0287	3.81E-07
	21	0.0433	5.84E-08	0.0300	9.55E-08	0.9756		0.0407	8.07E-08	0.0290	1.05E-07

on the DSC-Diffuser, suggesting that once a goal is defined, the system can infer the task with reduced need for external guidance, underscoring the efficiency of goal-oriented models.

- 3) The inclusion of goals enhances stability, realism, and generalization. Our DSC-Diffuser excels in learning from multi-task expert data, achieving low ADE and FDE without collisions, demonstrating strong generalization capabilities that allow adaptation across various driving tasks without compromising performance.
- 4) The integration of DHOCBF significantly enhances safety, improving SR values without sacrificing performance. This safety constraint ensures stability and reduces the risk of unsafe behavior, particularly in untrained environments.

The experiment conducted in this study demonstrates the stability, realism, and generalization of our proposed DSC-Diffuser planning method while maintaining driving safety. Our proposed method offers a promising approach for safe and adaptable autonomous driving. There exist some limitations. Our study assumes that other vehicles do not respond to the ego vehicle's actions, which is a significant limitation in autonomous driving planning [52]. It is also assumed that the sensory system can perfectly obtain the states of other vehicles, which could be improved by accounting for the prediction and uncertainty of other vehicles' states and limitations of the sensory system.

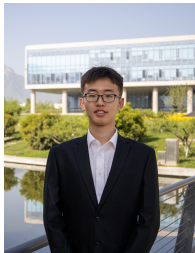
REFERENCES

- [1] National Highway Traffic Safety Administration (NHTSA). Unsignalized Intersection Crashes. <https://highways.dot.gov/safety/intersection-safety/about>, 2024. [Accessed 30-10-2024].
- [2] Zhiqian Qiao, Jeff Schneider, and John M Dolan. Behavior planning at urban intersections through hierarchical reinforcement learning. In *2021 IEEE International Conference on Robotics and Automation (ICRA)*, pages 2667–2673. IEEE, 2021.
- [3] Hong Shu, Teng Liu, Xingyu Mu, and Dongpu Cao. Driving tasks transfer using deep reinforcement learning for decision-making of autonomous vehicles in unsignalized intersection. *IEEE Transactions on Vehicular Technology*, 71(1):41–52, 2022.
- [4] Zhiqian Qiao, Katharina Muelling, John M. Dolan, Praveen Palanisamy, and Priyantha Mudalige. Automatically generated curriculum based reinforcement learning for autonomous vehicles in urban environment. In *2018 IEEE Intelligent Vehicles Symposium (IV)*, pages 1233–1238, 2018.
- [5] Shivesh Khaitan and John M. Dolan. State dropout-based curriculum reinforcement learning for self-driving at unsignalized intersections. In *2022 IEEE/RSJ International Conference on Intelligent Robots and Systems (IROS)*, pages 12219–12224, 2022.
- [6] Hyunki Seong, Chanyoung Jung, Seungwook Lee, and David Hyunchul Shim. Learning to drive at unsignalized intersections using attention-based deep reinforcement learning. In *2021 IEEE International Intelligent Transportation Systems Conference (ITSC)*, pages 559–566, 2021.
- [7] Elham Ahmadi, Alireza Olama, Rodrigo Castelan Carlson, and Eduardo Camponogara. Signal-free path-free intersection control for connected vehicles under automated driving. *IEEE Transactions on Intelligent Vehicles*, 2024.
- [8] Yiren Lu, Justin Fu, George Tucker, Xinlei Pan, Eli Bronstein, Rebecca Roelofs, Benjamin Sapp, Brandyn White, Aleksandra Faust, Shimon Whiteson, Dragomir Anguelov, and Sergey Levine. Imitation is not enough: Robustifying imitation with reinforcement learning for challenging driving scenarios. In *2023 IEEE/RSJ International Conference on Intelligent Robots and Systems (IROS)*, pages 7553–7560, 2023.
- [9] Mohammad Al-Sharman, Luc Edes, Bert Sun, Vishal Jayakumar, Mohamed A Daoud, Derek Rayside, and William Melek. Autonomous driving at unsignalized intersections: A review of decision-making challenges and reinforcement learning-based solutions. *arXiv preprint arXiv:2409.13144*, 2024.
- [10] Cheng Chi, Zhenjia Xu, Siyuan Feng, Eric Cousineau, Yilun Du, Benjamin Burchfiel, Russ Tedrake, and Shuran Song. Diffusion policy: Visuomotor policy learning via action diffusion. *The International Journal of Robotics Research*, page 02783649241273668, 2023.
- [11] Mrdjan Jankovic. Robust control barrier functions for constrained stabilization of nonlinear systems. *Automatica*, 96:359–367, 2018.
- [12] Zhuozhu Jian, Zihong Yan, Xuanang Lei, Zihong Lu, Bin Lan, Xueqian Wang, and Bin Liang. Dynamic control barrier function-based model predictive control to safety-critical obstacle-avoidance of mobile robot. In *2023 IEEE International Conference on Robotics and Automation (ICRA)*, pages 3679–3685, 2023.
- [13] Wei Xiao and Calin Belta. High-order control barrier functions. *IEEE Transactions on Automatic Control*, 67(7):3655–3662, 2022.

- [14] Wei Zhan, Liting Sun, Di Wang, Haojie Shi, Aubrey Clausse, Maximilian Naumann, Julius Kümmerle, Hendrik Königshof, Christoph Stiller, Arnaud de La Fortelle, and Masayoshi Tomizuka. INTER-ACTION Dataset: An INTERNATIONAL, Adversarial and Cooperative motion Dataset in Interactive Driving Scenarios with Semantic Maps. *arXiv:1910.03088 [cs, eess]*, 2019.
- [15] Mehdi Naderi, Panagiotis Tzafalos, and Markos Papageorgiou. Optimal control of automated vehicles crossing a lane-free signal-free intersection. In *2024 European Control Conference (ECC)*, pages 1415–1422, 2024.
- [16] Xinle Gong, Bowen Wang, and Sheng Liang. Collision-free cooperative motion planning and decision-making for connected and automated vehicles at unsignalized intersections. *IEEE Transactions on Systems, Man, and Cybernetics: Systems*, 54(5):2744–2756, 2024.
- [17] Robert Hult, Mario Zanon, Sebastien Gros, and Paolo Falcone. Optimal coordination of automated vehicles at intersections: Theory and experiments. *IEEE Transactions on Control Systems Technology*, 27(6):2510–2525, 2018.
- [18] Biao Xu, Shengbo Eben Li, Yougang Bian, Shen Li, Xuegang Jeff Ban, Jianqiang Wang, and Keqiang Li. Distributed conflict-free cooperation for multiple connected vehicles at unsignalized intersections. *Transportation Research Part C: Emerging Technologies*, 93:322–334, 2018.
- [19] Bowen Wang, Xinle Gong, Yafei Wang, Peiyuan Lyu, and Sheng Liang. Coordination for connected and autonomous vehicles at unsignalized intersections: An iterative learning-based collision-free motion planning method. *IEEE Internet of Things Journal*, 11(3):5439–5454, 2024.
- [20] Volkan Sezer, Tirthankar Bandyopadhyay, Daniela Rus, Emilio Frazzoli, and David Hsu. Towards autonomous navigation of unsignalized intersections under uncertainty of human driver intent. In *2015 IEEE/RSJ International Conference on Intelligent Robots and Systems (IROS)*, pages 3578–3585. IEEE, 2015.
- [21] Zhiqian Qiao, Katharina Muelling, John Dolan, Praveen Palanisamy, and Priyantha Mudalige. Pomdp and hierarchical options mdp with continuous actions for autonomous driving at intersections. In *2018 21st International Conference on Intelligent Transportation Systems (ITSC)*, pages 2377–2382, 2018.
- [22] Tommy Tram, Ivo Batkovic, Mohammad Ali, and Jonas Sjöberg. Learning when to drive in intersections by combining reinforcement learning and model predictive control. In *2019 IEEE Intelligent Transportation Systems Conference (ITSC)*, pages 3263–3268. IEEE, 2019.
- [23] Ethan Zhang, Ruixuan Zhang, and Neda Masoud. Predictive trajectory planning for autonomous vehicles at intersections using reinforcement learning. *Transportation Research Part C: Emerging Technologies*, 149:104063, 2023.
- [24] Mohammad Al-Sharman, Rowan Dempster, Mohamed A Daoud, Mahmoud Nasr, Derek Rayside, and William Melek. Self-learned autonomous driving at unsignalized intersections: A hierarchical reinforced learning approach for feasible decision-making. *IEEE Transactions on Intelligent Transportation Systems*, 24(11):12345–12356, 2023.
- [25] Di Chen, Meixin Zhu, Hao Yang, Xuesong Wang, and Yinhai Wang. Data-driven traffic simulation: A comprehensive review. *IEEE Transactions on Intelligent Vehicles*, 9(4):4730–4748, 2024.
- [26] Hesham M. Eraqi, Mohamed N. Moustafa, and Jens Honer. Dynamic conditional imitation learning for autonomous driving. *IEEE Transactions on Intelligent Transportation Systems*, 23(12):22988–23001, 2022.
- [27] Eli Bronstein, Mark Palatucci, Dominik Notz, Brandyn White, Alex Kuefler, Yiren Lu, Supratik Paul, Payam Nikdel, Paul Mougin, Hongge Chen, Justin Fu, Austin Abrams, Punit Shah, Evan Racah, Benjamin Frenkel, Shimon Whiteson, and Dragomir Anguelov. Hierarchical model-based imitation learning for planning in autonomous driving. In *2022 IEEE/RSJ International Conference on Intelligent Robots and Systems (IROS)*, pages 8652–8659, 2022.
- [28] Bikun Wang, Zhipeng Wang, Chenhao Zhu, Zhiqiang Zhang, Zhichen Wang, Penghong Lin, Jingchu Liu, and Qian Zhang. Interpretable motion planner for urban driving via hierarchical imitation learning. In *2023 IEEE/RSJ International Conference on Intelligent Robots and Systems (IROS)*, pages 1691–1696, 2023.
- [29] Zibin Dong, Yifu Yuan, Jianye Hao, Fei Ni, Yi Ma, Pengyi Li, and Yan Zheng. CleanDiffuser: An Easy-to-use Modularized Library for Diffusion Models in Decision Making, June 2024.
- [30] Brian Yang, Huangyuan Su, Nikolaos Gkanatsios, Tsung-Wei Ke, Ayush Jain, Jeff Schneider, and Katerina Fragkiadaki. Diffusion-es: Gradient-free planning with diffusion for autonomous driving and zero-shot instruction following. *arXiv preprint arXiv:2402.06559*, 2024.
- [31] Haoran He, Chenjia Bai, Kang Xu, Zhuoran Yang, Weinan Zhang, Dong Wang, Bin Zhao, and Xuelong Li. Diffusion model is an effective planner and data synthesizer for multi-task reinforcement learning. *Advances in neural information processing systems*, 36, 2024.
- [32] Chen Liu, Shibo He, Haoyu Liu, and Jiming Chen. Intention-aware denoising diffusion model for trajectory prediction. *arXiv preprint arXiv:2403.09190*, 2024.
- [33] Mitchell Black, Mrdjan Jankovic, Abhishek Sharma, and Dimitra Panagou. Future-focused control barrier functions for autonomous vehicle control. In *2023 American Control Conference (ACC)*, pages 3324–3331, 2023.
- [34] Joohwan Seo, Joonho Lee, Eunkyoo Baek, Roberto Horowitz, and Jongeun Choi. Safety-critical control with nonaffine control inputs via a relaxed control barrier function for an autonomous vehicle. *IEEE Robotics and Automation Letters*, 7(2):1944–1951, 2022.
- [35] Yiwei Lyu, Wenhao Luo, and John M. Dolan. Adaptive safe merging control for heterogeneous autonomous vehicles using parametric control barrier functions. In *2022 IEEE Intelligent Vehicles Symposium (IV)*, pages 542–547, 2022.
- [36] Kota Kondo, Andrea Tagliabue, Xiaoyi Cai, Claudius Tewari, Olivia Garcia, Marcos Espitia-Alvarez, and Jonathan P How. Cgd: Constraint-guided diffusion policies for uav trajectory planning. *arXiv preprint arXiv:2405.01758*, 2024.
- [37] Wei Xiao, Tsun-Hsuan Wang, Chuang Gan, and Daniela Rus. Safediffuser: Safe planning with diffusion probabilistic models. *arXiv preprint arXiv:2306.00148*, 2023.
- [38] Kywoon Lee, Seongun Kim, and Jaesik Choi. Refining diffusion planner for reliable behavior synthesis by automatic detection of infeasible plans. *Advances in Neural Information Processing Systems*, 36, 2024.
- [39] Zhengyu Hou, Wenjun Liu, and Alois Knoll. Safe reinforcement learning for autonomous driving by using disturbance-observer-based control barrier functions. *IEEE Transactions on Intelligent Vehicles*, pages 1–10, 2024.
- [40] Jingyuan Zhou, Longhao Yan, and Kaidi Yang. Enhancing system-level safety in mixed-autonomy platoon via safe reinforcement learning. *IEEE Transactions on Intelligent Vehicles*, 2024.
- [41] Rafael Vivacqua, Raquel Vassallo, and Felipe Martins. A low cost sensors approach for accurate vehicle localization and autonomous driving application. *Sensors*, 17(10):2359, 2017.
- [42] Jonathan Ho, Ajay Jain, and Pieter Abbeel. Denoising diffusion probabilistic models. *Advances in neural information processing systems*, 33:6840–6851, 2020.
- [43] Jonathan Ho and Tim Salimans. Classifier-free diffusion guidance. *arXiv preprint arXiv:2207.12598*, 2022.
- [44] Michael Janner, Yilun Du, Joshua B Tenenbaum, and Sergey Levine. Planning with diffusion for flexible behavior synthesis. *arXiv preprint arXiv:2205.09991*, 2022.
- [45] Aaron D Ames, Jessy W Grizzle, and Paulo Tabuada. Control barrier function based quadratic programs with application to adaptive cruise control. In *53rd IEEE conference on decision and control*, pages 6271–6278. IEEE, 2014.
- [46] Akshay Thirugnanam, Jun Zeng, and Koushil Sreenath. Safety-critical control and planning for obstacle avoidance between polytopes with control barrier functions. In *2022 International Conference on Robotics and Automation (ICRA)*, pages 286–292. IEEE, 2022.
- [47] Wei Xiao and Calin Belta. Control barrier functions for systems with high relative degree. In *2019 IEEE 58th conference on decision and control (CDC)*, pages 474–479. IEEE, 2019.
- [48] Aree Jamgochian, Etienne Buehrle, Johannes Fischer, and Mykel J Kochenderfer. Shail: Safety-aware hierarchical adversarial imitation learning for autonomous driving in urban environments. In *2023 IEEE International Conference on Robotics and Automation (ICRA)*, pages 1530–1536. IEEE, 2023.
- [49] Saleh Albeaik, Alexandre Bayen, Maria Teresa Chiri, Xiaoqian Gong, Amaury Hayat, Nicolas Kardous, Alexander Keimer, Sean T McQuade, Benedetto Piccoli, and Yiling You. Limitations and improvements of the intelligent driver model (idm). *SIAM Journal on Applied Dynamical Systems*, 21(3):1862–1892, 2022.
- [50] Faraz Torabi, Garrett Warnell, and Peter Stone. Behavioral cloning from observation. *arXiv preprint arXiv:1805.01954*, 2018.
- [51] Jonathan Ho and Stefano Ermon. Generative adversarial imitation learning. *Advances in neural information processing systems*, 29, 2016.
- [52] Nicholas Rhinehart, Jeff He, Charles Packer, Matthew A Wright, Rowan McAllister, Joseph E Gonzalez, and Sergey Levine. Contingencies from observations: Tractable contingency planning with learned behavior models. In *2021 IEEE International Conference on Robotics and Automation (ICRA)*, pages 13663–13669. IEEE, 2021.



Di Chen received the B.Sc. and M.S. degree in Transportation Engineering from School of Transportation engineering, Tongji University, Shanghai, China. She is a research assistant in the Department of Electrical and Electronic Engineering of The Hong Kong Polytechnic University. Her research interests include traffic simulation, machine learning methods for intelligent transportation.



Ruiguo Zhong received the B.Sc. and M.S. degree in Control Science and Engineering from School of Electronics and Information, Northwestern Polytechnical University, Shaanxi, China. Currently, he is a Ph.D. student in the Hong Kong University of Science and Technology (Guangzhou), China. His research interests include generative methods for intelligent transportation.



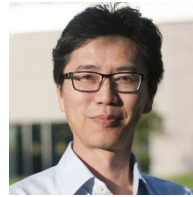
Kehua Chen received a B.S. degree in civil engineering from Chongqing University, a dual M.S. degree in Environmental Science from both University of Chinese Academy of Sciences and University of Copenhagen, and is now a Ph.D. student with the Division of Emerging Interdisciplinary Areas, Hong Kong University of Science and Technology. His research interests include spatial-temporal data mining, urban computing, driver behavior analysis and modeling.



Zhiwei Shang received the B.S. degree in Hydrology and Water Resources Engineering from the Sichuan University, China, in 2020, and the M.S. degree in Computer Technology from University of Chinese Academy of Sciences, China, in 2023. Currently, he is a research assistant at the Hong Kong University of Science and Technology (Guangzhou), China. His research interests mainly include reinforcement learning and intelligent control.



Meixin Zhu is a tenure-track Assistant Professor in the Thrust of Intelligent Transportation (INTR) under the Systems Hub at the Hong Kong University of Science and Technology (Guangzhou). He is also an affiliated Assistant Professor in the Civil and Environmental Engineering Department at the Hong Kong University of Science and Technology. He obtained a Ph.D. degree in intelligent transportation at the University of Washington (UW) in 2022. He received his B.S. and M.S. degrees in traffic engineering in 2015 and 2018, respectively, from Tongji University. His research interests include Autonomous Driving Decision Making and Planning, Driving Behavior Modeling, Traffic-Flow Modeling and Simulation, Traffic Signal Control, and (Multi-Agent) Reinforcement Learning. He is a recipient of the TRB Best Dissertation Award (AED50) in 2023.



Edward Chung is a Professor of Intelligent Transport Systems (ITS) at the Department of Electrical Electronic Engineering of The Hong Kong Polytechnic University. Edward received a Bachelor of Civil Engineering with Honours and PhD from Monash University. With an extensive background as both an engineer and an accomplished academic researcher, Edward has garnered significant experience working on national and international projects. Notably, he held positions such as Senior Research Scientist at the Australian Road Research Board, Manager of Infrastructure Analysis and Modelling at the Victorian Department of Infrastructure, Australia, Visiting Professor at the Centre for Collaborative Research, University of Tokyo, and Head of the ITS Group at LAVOC, EPFL, Switzerland. Prior to his current role at PolyU, Edward served as a professor at the Queensland University of Technology (QUT) and held the position of Director of the Smart Transport Research Centre at QUT.